End-to-End Color Printer Calibration by Total Least Squares Regression

Minghui Xia, Eli Saber, *Member, IEEE,* Gaurav Sharma, *Member, IEEE,* and A. Murat Tekalp, *Senior Member, IEEE*

***Abstract*— Neugebauer modeling plays an important role in obtaining end-to-end device characterization profiles for halftone color printer calibration. This paper proposes total least square (TLS) regression methods to estimate the parameters of various Neugebauer models. Compared to the traditional least squares (LS) based methods, the TLS approach is physically more appropriate for the printer modeling problem because it accounts for errors in the measured reflectance of both the primaries and the modeled samples. A TLS method based on print measurements from single-colorant step-wedges is first developed. The method is then extended to incorporate multicolorant print measurements using an iterative algorithm. The LS and TLS techniques are compared through tests performed on two color printers, one employing conventional rotated halftone screens and the other using a dot-on-dot halftone screen configuration. Our experiments indicate that the TLS methods yield a consistent and significant improvement over the LS-based techniques for model parameter estimation. The gains from the TLS method are particularly significant when the number of patches for which measured data is available is limited.**

***Index Terms*— Color printer calibration, halftone color, least squares, Neugebauer model, total least squares.**

I. Introduction

RECENT years have seen a proliferation of color imaging devices in home and office environments. Consequently, color imaging is an active area of research and development (see [1] for a recent survey). In order to obtain accurate color, the different devices need to be calibrated. The native color representations of common color imaging devices are very different and highly *device dependent*. In order to utilize color effectively in networked, open-systems environments, it is necessary to calibrate these devices to *device independent* (DVI) standards, such as the standards defined by the International Commission on Illumination (CIE) [2] for unambiguous measurement and communication of color. Thus, input devices, such as color scanners and cameras, must be calibrated to obtain DVI color values from their measurements; and output devices, such as monitor displays and printers, need to be calibrated so that the digital control values required to produce a given DVI color can be readily determined. For the purposes of this paper, we will assume that the reader is familiar with basic terms in color imaging systems. An extensive overview of color science terms and concepts can be found in [1] and [3]–[6].

In general, the calibration of a color output device is a two-step process. In the first step, one determines a device characterization function, which represents the output device as an abstract mapping from a set of digital control values to colors specified in a DVI color space. This device characterization function is then inverted, so that the digital control values required to produce a given color (specified in a DVI color space) may be computed. Details of the inversion process can be found in [7] and [8]. This paper focuses on a specific instance of the first step, i.e., the characterization of halftone color printers (see [1] for a brief description of different types of color printers). Typically, these printers are binary devices that have the capability of putting one or more of cyan (C), magenta (M), yellow (Y), and black (K) colorants on each addressable pixel on paper. Due to the spatial lowpass characteristics of the human eye, the perceived color is a spatial average of the mosaic of colors produced on the paper. The process of obtaining pixel bitmaps for printing images is known as halftoning and is an active area of independent research. The interested reader is referred to [1] and [9]–[11] for comprehensive reviews of halftoning algorithms. A halftone printer can be calibrated at the pixel level [12]–[15] or from end to end with the halftoning algorithm viewed as a black box (see Fig. 1). The latter approach requires a separate calibration for each halftoning scheme used. However, the first approach requires complete control of the binary patterns being printed, which is often not feasible. Therefore, the latter approach will be considered in this paper.

Since the device characterization function for color halftone printers is highly nonlinear, a large number of sample measurements are required for a purely interpolation based empirical representation of the characterization function. Consequently, printer models based on the physics of the color printing process therefore offer an attractive alternative for characterization, where the model parameters can often be determined from a small number of measurements. A physical model for the halftone printing process was first proposed by Neuge-

Manuscript received November 5, 1997; revised June 16, 1998. This work was supported by the Invention Opportunity Program Committee and the Production Controller Software Development Team of Xerox Corporation. The associate editor coordinating the review of this manuscript and approving it for publication was Prof. Brian Funt.

M. Xia is with Information Sciences and Systems, Department of Electrical Engineering, Princeton University, Princeton, NJ 08544 USA (e-mail: xia@ee.princeton.edu).

E. Saber is with Print Engine Delivery Unit, Xerox Corporation, Webster, NY 14580 USA (e-mail: eli.saber@usa.xerox.com).

G. Sharma is with the Digital Imaging Technology Center, Xerox Corporation, Webster, NY 14580 USA (e-mail: sharma@wrc.xerox.com).

A. M. Tekalp is with the Department of Electrical Engineering and Center for Electronic Imaging Systems, University of Rochester, Rochester, NY 14627 USA (e-mail: tekalp@ee.rochester.edu).

Publisher Item Identifier S 1057-7149(99)03426-0.

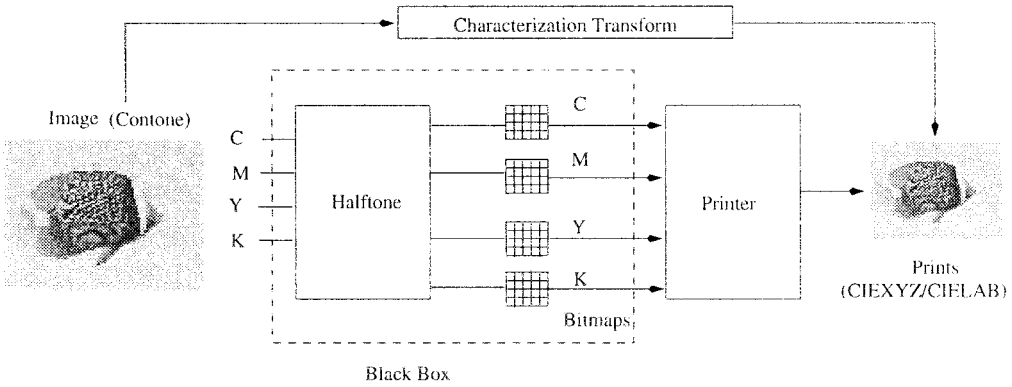

Fig. 1. End-to-end printer characterization where the halftoning process is treated as a black box.

bauer in 1937 [16]. Recently, significant improvements to this model have been achieved by the introduction of the Yule–Nielsen (YN) correction factor n [17], [18] and the spectral Neugebauer model [19], [20]. In [20], the model parameters are estimated by a global search technique to minimize a predefined model prediction error. Although the search provides satisfactory results, it is computationally expensive. An alternative approach is to perform the optimization by least squares estimation [21], where the parameters are obtained by solving a set of overdetermined linear equations. Implicit within the least square method is the assumption that only the measurements of the training sets are subject to error, while the Neugebauer primaries are free of error. A more realistic model of the physical process can be obtained by allowing both the primaries and training sets to contain measurement errors, which necessitates the total least squares estimation of the model parameters.

This paper proposes total least squares (TLS) regression methods to estimate the model parameters in the presence of measurement errors in both the Neugebauer primaries and the print samples constituting the training sets. The technique is applied to random and the dot-on-dot mixing models, where for each case the analysis is performed by employing single, multicolorant, and gray type step-wedges as well as a combination of all of the above with additional multicolorant step-wedges. The results indicate that the TLS based algorithms provide a more accurate parameter estimation than the LS-based techniques. The remainder of this paper is organized as follows. Neugebauer modeling for rotated and dot-on-dot screens and the TLS technique are briefly reviewed in Section II. The proposed algorithms for printer modeling and parameter estimation are presented in Section III. Experimental results are discussed in Section IV, and conclusions are drawn in Section V.

II. Background

A. Neugebauer Models

In halftone printing using CMYK colorants, up to $2^4 = 16$ different colored regions or primaries are produced on paper through subtractive overlap of one, two, three, four, or no colorants. Neugebauer was the first to suggest that halftone reproduction may be viewed as an additive process involving these primaries, which are now referred to as the *Neugebauer primaries*. In his original model, tristimulus of a halftone print was expressed as the weighted average of the tristimuli of the individual primaries, with the weighting factor of each primary given by its fractional area. Recently, considerable success has been obtained by utilizing a spectral Neugebauer model [19], [20]. The spectral model improvements are obtained by expressing the macroreflectance (instead of tristimuli) of a halftoned region as the weighted average of the microreflectance of the individual Neugebauer primaries:[1]

$$r(\lambda;\mathbf{w}) = \sum_{i=1}^{P} w_i r_i(\lambda) \tag{1}$$

where λ denotes the wavelength of light, P is the number of Neugebauer primaries (for a typical CMYK printer, $P = 16$), $r(\lambda;\mathbf{w})$ is the predicted spectral reflectance corresponding to a halftone print with fractional areas of the Neugebauer primaries given by $\mathbf{w} = [w_1, w_2, \cdots w_P]$, w_i is the fractional area of the ith Neugebauer primary, and $r_i(\lambda)$ is the reflectance of the ith primary. It should be noted that since the areas of the primaries are expressed as fractions of the total area over which the average macroreflectance is computed, they satisfy the constraint $\sum_{i=1}^{P} w_i = 1$.

Due to the penetration and scattering of light in paper known as the *Yule–Nielsen effect* [17], [18], the basic model (1) does not perform well in practice. Fortunately, an added empirical correction has yielded significant improvements [22].[2] The spectral Neugebauer model with the so-called YN correction is

$$r^{1/n}(\lambda;\mathbf{w}) = \sum_{i=1}^{P} w_i r_i^{1/n}(\lambda) \tag{2}$$

where n represents the YN correction factor. In theory, n varies between one and two, corresponding to the two extremes of no scattering of light in paper and complete Lambertian scattering. However, the introduction of a general value for n

[1] Note that the term *macroreflectance* has been used here to indicate that this is an average reflectance over a region composed of different microreflectances.

[2] This modification was originally suggested for black and white halftone printing by Yule and Nielsen [17], and later applied to tristimulus data. It was extended to the case of the spectral model by Viggiano [19].

is a purely empirical modification of the equations to better approximate the physical measurements. Like other researchers [19], [23], we have discovered that values larger than two often provide better agreement with the data. Therefore, n is treated as a free parameter and allowed to vary over a wider range of values to obtain the best agreement with the measured color data.

1) Random Mixing and Demichel Equations: The use of the Neugebauer model requires establishing a relationship between the digital C, M, Y, and K control values that drive the printer and the fractional areas of the Neugebauer primaries $\{w_i\}_{i=1}^{P}$. This relationship depends on the nature of the interactions between the colorants in the printer. If the separations are printed independently and the overlap between the separations is random (called *random mixing*), the fractional areas corresponding to the primaries can be determined by a probabilistic model first proposed by Demichel [24] as

$$\begin{aligned} w_i \in \{&(1-c)(1-m)(1-y)(1-k),(1-c)(1-m)\\ &\times(1-y)k,(1-c)(1-m)y(1-k),(1-c)(1-m)yk,\\ &(1-c)m(1-y)(1-k),(1-c)m(1-y)k,\\ &(1-c)my(1-k),(1-c)myk,c(1-m)(1-y)\\ &\times(1-k),c(1-m)(1-y)k,c(1-m)y(1-k),\\ &c(1-m)yk,cm(1-y)(1-k),cm(1-y)k,\\ &cmy(1-k),cmyk\} \end{aligned} \tag{3}$$

where c, m, y, and k represent the fractional areas covered by the C, M, Y, and K colorants, respectively. The relationship between the actual dot areas c, m, y, k and the digital control values C, M, Y, K is usually nonlinear, and is often referred to as the *dot growth function* or *dot area function*.

It is common to independently halftone the C, M, Y, and K separations using rotated screens to closely approximate the random overlap assumed in the Demichel equations. The main reason for the use of rotated screens is their relative insensitivity to interseparation registration errors, which are frequently encountered in color printing systems. The process of characterization of the printer is then reduced to the problem of relating the dot areas c, m, y, and k to the corresponding digital values C, M, Y, and K. It should be noted that the Demichel equations are inappropriate for certain types of printing systems—such as inkjet printers which restrict the amount of ink at each pixel location—and special halftoning algorithms that work on all color separations together (vector error-diffusion); while the Neugebauer model remains a physically valid model for several of these cases.

2) Dot-on-Dot Mixing: The Demichel equation (3) does not accurately describe the characteristics of halftone printers which employ a dot-on-dot (or line-on-line) screen. In a dot-on-dot screen, the halftone dots of the different colorants are aligned so as to maximize the overlap between the colorants. For such a halftoning scheme, it can be seen that for a given region of the device color space (specified by the CMYK values), at most five of the 16 total primaries are active [23]. Fig. 2 shows an example of the arrangement of dots for a dot-on-dot halftone printer with four colorants for a region of color space, where the colorants in decreasing order of ink coverages are C, M, Y, and K, respectively. It is obvious that only five primaries C, CM, CMY, CMYK, and W (paper white) are present in this example (note that the specification of the primaries depends on the order of the C, M, Y, and K ink coverage). If we let p_1, p_2, p_3, p_4 denote the printer colorants in increasing dot area coverage, and a_1, a_2, a_3, a_4 the corresponding dot areas, (2) can be rewritten as [23]

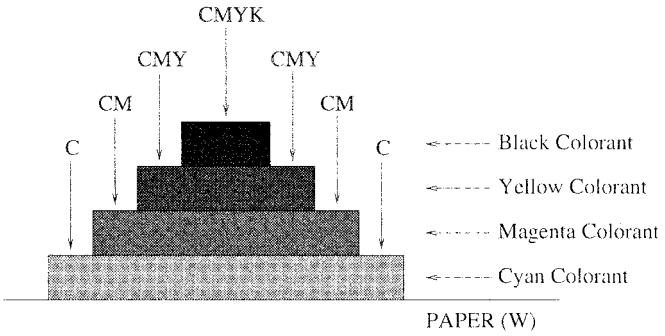

Fig. 2. Example of dot-on-dot screen configuration.

$$r^{1/n}(\lambda) = \sum_{i=1}^{5} w_i {r_i}^{1/n}(\lambda) \tag{4}$$

where $r_i \in \{r_{p_1p_2p_3p_4}(\lambda), r_{p_2p_3p_4}(\lambda), r_{p_3p_4}(\lambda), r_{p_4}(\lambda), r_w(\lambda)\}$ denote the five primaries, and $w_i \in \{a_1, a_2 - a_1, a_3 - a_2, a_4 - a_3, 1 - a_4\}$ are the corresponding fractional areas. Note that while only five primaries are used in the dot-on-dot model in a given region of CMYK values, the specific primaries used are different in different regions of the CMYK space, and all 16 primaries are still required to model the printer.

The dot-on-dot mixing model assumes an ideal dot pattern with no noise and no misregistration effects. These assumptions are generally not valid in all practical cases. Therefore, a combination of the dot-on-dot (4) and the random mixing model (2) is introduced in [23] to improve the prediction accuracy. The combined model represents the predicted reflectance as

$$r(\lambda) = (1-\alpha) r_d(\lambda) + \alpha r_r(\lambda) \tag{5}$$

where $r_d(\lambda)$ is the reflectance predicted by the dot-on-dot model (4), $r_r(\lambda)$ is the reflectance predicted by the random mixing model (2), and α is a "noise factor" (within the range of $(0, 1)$) which determines the relative contributions of the two models to the mixing process.

3) Parameter Estimation of Neugebauer Models: In order to use the Neugebauer model to characterize a halftone printer, it is necessary to estimate the model parameters, i.e., the primary reflectance functions, the CMYK dot growth functions, the YN correction factor, and (if applicable) the noise factor. Since these parameters are not known *a-priori* and their values differ significantly among various printers, they are determined from measurements of print samples produced by the device. Traditionally, the primary reflectance functions are obtained from direct measurements, while the other parameters are estimated using linear least-squares or other optimization methods. These methods tend to ignore

the noise in the measurements of the primaries themselves, which could contribute to significant error in the model. The main contribution of this paper is to propose new TLS regression methods for estimating primary reflectance and dot growth functions based on a more realistic physical model. The YN correction parameter n and the noise factor α are estimated by iterating through a set of candidate values within empirically established boundaries. For these parameters, the values leading to the smallest prediction error is selected as the optimum.

B. Total Least Squares (TLS) Method

Given an overdetermined set of m linear equations $Ax \approx b$ in n unknowns x, the well-known LS method finds a solution x which

$$\text{minimizes } \|b - \hat{b}\| \quad \text{subject to } \hat{A}x = \hat{b} \tag{6}$$

while the TLS method seeks to find a solution x which

$$\text{minimizes } \|[A; b] - [\hat{A}; \hat{b}]\|_F \quad \text{subject to } \hat{A}x = \hat{b} \tag{7}$$

where 'F' denotes the Frobenius norm [25]. Any x satisfying $\hat{A}x = \hat{b}$ is called a TLS solution and $[\Delta\hat{A}; \Delta\hat{b}] = [A; b] - [\hat{A}; \hat{b}]$ is the corresponding TLS correction. The TLS solution is computed through singular value decomposition (SVD). Details of this technique along with an extensive discussion of TLS and its statistical properties can be found in [26].

If more than one right-hand side vector are observed and are associated with the same parameter matrix A, the TLS problem becomes multidimensional. Specifically, we are given a set of equations $AX \approx B$ where B is a $m \times d$ observations matrix, A is a $m \times n$ parameter matrix and X has $n \times d$ unknowns. The multidimensional TLS problem seeks to

$$\text{minimize } \|[A; B] - [\hat{A}; \hat{B}]\|_F \quad \text{subject to } \hat{A}X = \hat{B}; \quad [\hat{A}; \hat{B}] \in \Re^{m \times (n+d)}. \tag{8}$$

X is called a TLS solution denoted by $\hat{X}_{\text{TLS}}$ and $[\Delta\hat{A}; \Delta\hat{B}] = [A; B] - [\hat{A}; \hat{B}]$ is the corresponding TLS correction. Again, the problem can be solved by employing SVD-based techniques [26]. In fact, the one dimensional TLS problem in (7) represents a special case of the multidimensional TLS problem in (8). As will be apparent from the following sections, both single and multidimensional problems are encountered in the problem of printer characterization using Neugebauer models.

A geometric interpretation of LS and TLS provides useful insight in understanding the difference between them. In solving an overdetermined system, the initial set of equations $Ax \approx b$ is inconsistent. Geometrically, this implies that the n-dimensional subspace $\Re(A)$ of $\Re^m$, generated by the columns of A, does not contain b. The best "least-square" approximation b' is then the orthogonal projection of b onto that subspace. In many applications, both A and b are subject to errors. It is then inappropriate to "correct" only b. Thus, TLS seeks to "bend" both b and the set of columns a_i of A toward each other until the new set of equations is consistent. Furthermore, all correction vectors $\Delta\hat{a}_i$ and $\Delta\hat{b}_i$ applied to the columns of A and b are minimized according to (7).

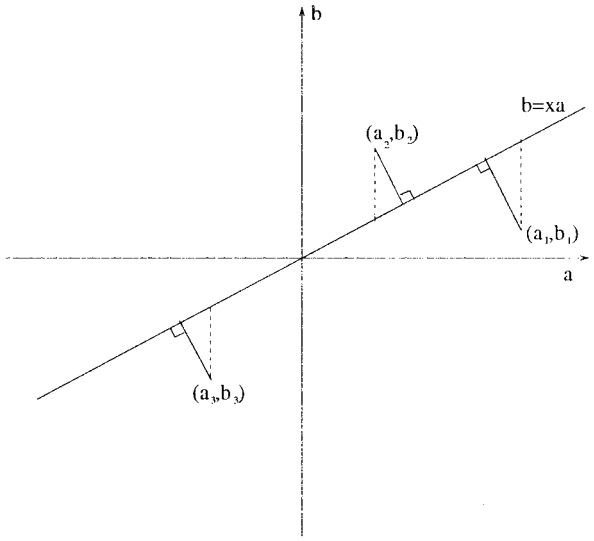

Fig. 3. LS versus TLS. The dashed lines denote LS error and the solid lines perpendicular to line $b = xa$ denote TLS error.

Fig. 3 illustrates graphically the difference between the one dimensional LS and TLS case. The LS method minimizes the squared sum of the vertical distances; whereas the TLS method minimizes the squared sum of the perpendicular distances.

III. Total Least Squares Regression for Printer Modeling

A. Modeling Measurement Errors

The spectral Neugebauer model with YN correction (2) ignores measurement errors in the reflectances of the primaries, $\{r_i(\lambda)\}$. A more accurate model that allows errors in all measured quantities is

$$r^{1/n}(\lambda; \mathbf{w}) + e(\lambda) = \sum_{i=1}^{P} w_i \left[r_i^{1/n}(\lambda) + e_i(\lambda)\right] \tag{9}$$

where $e(\lambda)$ denotes the measurement and model errors in the YN-corrected spectral space, and $e_i(\lambda)$ is the error in the YN-corrected measured reflectance of the ith primary.

In order to apply the TLS method to the printer modeling problem, the unity sum constraint on the fractional areas of the primaries, e.g., $\sum_{i=1}^{P} w_i = 1$, must be incorporated into (9). To this effect, we assume without loss of generality that the first Neugebauer primary, $r_1(\lambda)$, corresponds to paper white reflectance. Then, subtracting $r_1^{1/n}(\lambda)$ from both sides, (9) can be rewritten as

$$\left[r^{1/n}(\lambda; \mathbf{w}) - r_1^{1/n}(\lambda)\right] + e(\lambda) = \sum_{i=1}^{P} w_i \left[r_i{}^{1/n}(\lambda) + e_i(\lambda)\right] - \left(\sum_{i=1}^{P} w_i\right) r_1^{1/n}(\lambda) \tag{10}$$

and rearranged as

$$\left[r^{1/n}(\lambda; \mathbf{w}) - r_1^{1/n}(\lambda)\right] + e(\lambda) = \sum_{i=2}^{P} w_i \left[r_i{}^{1/n}(\lambda) - r_1^{1/n}(\lambda) + e_i(\lambda)\right] + w_1 e_1(\lambda) \tag{11}$$

yielding

$$r'(\lambda;\mathbf{w}')+e'(\lambda)=\sum_{i=2}^{P}w_i(r'_i(\lambda)+e_i(\lambda)) \tag{12}$$

where

$$\mathbf{w}'=[w_2,w_3,\dots w_p]^T,\quad r'_i(\lambda)=r_i^{1/n}(\lambda)-r_1^{1/n}(\lambda),$$
$$r'(\lambda;\mathbf{w}')=r^{1/n}(\lambda;\mathbf{w})-r_1^{1/n}(\lambda),$$
$$e'(\lambda)=e(\lambda)-w_1e_1(\lambda).$$

Typically, the color spectra are sampled at discrete wavelengths, $[\lambda_1,\lambda_2,\cdots\lambda_N]$, so that (12) can be written in matrix-vector notation as

$$\mathbf{r}'(\mathbf{w}')+\mathbf{e}'=\sum_{i=2}^{P}w_i(\mathbf{r}'_i+\mathbf{e}_i)=(\mathbf{R}'_p+\mathbf{E})\mathbf{w}' \tag{13}$$

where

$$\mathbf{r}'=[r'(\lambda_1;\mathbf{w}'),\cdots r'(\lambda_N;\mathbf{w}')]^T,$$
$$\mathbf{e}'=[e'(\lambda_1),\cdots e'(\lambda_N)]^T,$$
$$\mathbf{r}'_i=[r'_i(\lambda_1),\cdots r'_i(\lambda_N)]^T,$$
$$\mathbf{e}_i=[e_i(\lambda_1),\cdots e_i(\lambda_N)]^T,$$
$$\mathbf{R}'_p=[\mathbf{r}'_2,\mathbf{r}'_3\cdots\mathbf{r}'_P],$$
$$\mathbf{E}=[\mathbf{e}_2,\mathbf{e}_3,\cdots\mathbf{e}_P].$$

The vector $\mathbf{r}'$ represents the YN-corrected and paper "normalized" reflectance. We will adhere to this convention of using primed vectors for YN-corrected and paper-normalized reflectance throughout this paper. To avoid needless repetition of the "YN-corrected and paper normalized" qualifier, we will simply refer to these terms as "reflectance" hereafter.

The above equations follow the multidimensional TLS data model in Section II-B. Therefore, the areas of the Neugebauer primaries w_i and the correction $\mathbf{E}$ to the primary reflectance can be simultaneously obtained by solving (13).[3] However, such a scheme has limited utility because the areas of the Neugebauer primaries, w_i, are usually interdependent variables that are related to each other by means of the mixing equations discussed in Section II-A1 and II-A2. The independent variables are actually the fractional areas of the single-colorants in terms of which the primary areas w_i are expressed. The incorporation of the mixing equations into (13) makes these equations nonlinear and intractable for the TLS method. An interesting special case for which the equations remain linear occurs when the prints have only one colorant.

B. TLS for Single-Colorant Step-Wedges

The TLS method can be used to obtain the dot growth function from single-colorant prints. Usually, these prints are in a sequence with the (fractional) colorant coverage on the paper increasing monotonically from zero to one. The prints are generated by stepping through the digital values used for driving the printer, typically from zero to 255, and are therefore referred to as step-wedges. Since there is only one colorant in this case, a simplified Neugebauer model with only two primaries (one colorant and paper white) is applicable. Thus, for a K-step cyan wedge, with digital values $0\le C_1\le\cdots\le C_K\le 255$, (13) reduces to

$$(\mathbf{r}'_{\rm pc}+\mathbf{e}'_{\rm pc})c_j=\mathbf{r}'_{c_j}+\mathbf{e}'_{c_j},\quad j=1,2,\cdots K \tag{14}$$

where c_j denotes the dot area corresponding to the digital step value C_j, $\mathbf{r}'_{\rm pc}$ denotes the cyan primary reflectance, $\mathbf{r}'_{c_j}$ denotes the reflectance of the jth step, $\mathbf{e}'_{c_j}$, and $\mathbf{e}'_{\rm pc}$ denotes the measurement error in $\mathbf{r}'_{c_j}$ and $\mathbf{r}'_{\rm pc}$, respectively. The K equations in (14) may be combined as

$$(\mathbf{r}'_{\rm pc}+\mathbf{e}'_{\rm pc})\mathbf{c}^T=\mathbf{R}'_c+\mathbf{E}'_c \tag{15}$$

where $\mathbf{c}=[c_1,c_2,\dots c_K]^T$, $\mathbf{R}'_c=[\mathbf{r}'_{c_1},\mathbf{r}'_{c_2},\dots\mathbf{r}'_{c_K}]$, and $\mathbf{E}'_c=[\mathbf{e}'_{c_1},\mathbf{e}'_{c_2},\dots\mathbf{e}'_{c_K}]$.

Observing that the above equations represent a multidimensional TLS problem, we can "solve" them following the approach in Section II-B, to obtain simultaneously the dot areas of cyan $\mathbf{c}$ and the correction $\mathbf{e}'_{\rm pc}$ to the cyan primary reflectance. Note that one could potentially solve (14) as a one-dimensional (1-D) TLS problem. Since all the "observation data" $\mathbf{r}'_{c_j}$ are associated with one primary reflectance $\mathbf{r}'_{\rm pc}$, a better solution can be obtained by combining the data of all steps for cyan.

The multidimensional TLS regression procedure described above determines corrections for the cyan primary reflectance and a correspondence between the digital values C_j and the fractional area coverage c_j. For intermediate digital values, the conversion from digital values to fractional colorant area coverage may be obtained by interpolation. The same approach can be applied to magenta, yellow, and black step-wedges to obtain the corresponding dot growth functions. The random, dot-on-dot, or combined mixing equations may then be used to obtain the fractional areas of the Neugebauer primaries for prints having more than one colorant, which in turn can be used to predict the reflectance from the model in (2). The complete printer model based on this approach is shown in Fig. 4. Note that this approach assumes that different colorants are independent in that the fractional area coverage of a colorant depends only on the digital value of that colorant and is independent of the digital values of the other colorants. This assumption is reasonable in a vast majority of color halftone printers that print the C, M, Y, and K separations independently, but is not valid for printers in which the printing of separations is interdependent.

One limitation of the printer characterization scheme described above is that the model parameters are determined only based on single-colorant prints even though the model is used for both single and multicolorant prints. More robust estimates could potentially be obtained by using multicolorant prints in the estimation process. As mentioned earlier, if the complete problem is considered in the most general case, the model is nonlinear in the model parameters, and the optimal parameters cannot be readily estimated. However, if initial estimates of the model parameters are available, some multicolorant prints can be used to refine these estimates. Several such schemes are

[3] If the measurement noise term affecting the primaries (the matrix $\mathbf{E}$) is ignored, then simple least squares regression can be employed to estimate the dot growth function [21].

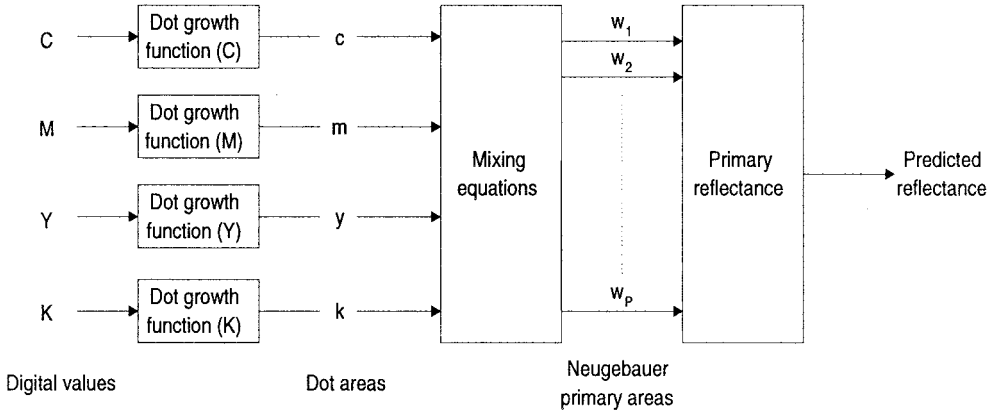

Fig. 4. Diagram of overall printer model.

considered for the random mixing model and the dot-on-dot mixing model in the following sections.

C. TLS for the Random Mixing Model with Selected Primary Updates

Here, we restrict ourselves to printers for which the random mixing model is applicable and consider the use of multicolorant prints to refine the dot growth functions estimated from the single-colorant step-wedges and update selected primary reflectances. Two kinds of multicolorant prints will be considered for the refinement procedure: 1) multicolorant step-wedges, which contain sweeps of one colorant (in digital value) with the other colorants held constant; and 2) gray step-wedge, which has no K colorant and equal digital values for the C, M, and Y colorants.

1) Refinement Using Multicolorant Step-Wedges: The dot growth functions estimated from single-colorant step-wedges can be iteratively refined, one colorant at a time, by using multicolorant step-wedges in which the dot areas of other colorants are known and assumed fixed. In order to illustrate the procedure, consider the process of refining the dot areas for the cyan colorant using a multicolorant cyan step-wedge. Suppose the cyan digital values for this multicolorant step-wedge are $0 \leq C_1 \leq C_2 \cdots \leq C_K \leq 255$ and the digital values (and therefore fractional areas) of other colorants are constant. The Neugebauer equations (2) can be used to model the reflectance of the multicolorant step-wedge prints, where fractional areas are given by Demichel equations (3). In the resulting equations, on the right hand side of (13), we can group together the terms with the factor c (these correspond to primaries that include the cyan colorant) and other terms with the factor $(1-c)$ (these correspond to primaries that do not include the cyan colorant), to get

$$\mathbf{r}^{\star\prime}_{c_j} + \mathbf{e}^{\star\prime}_{c_j} = c_j \sum_{k \in S_C} w^{\star}_k \left(\mathbf{r}'_{p_k} + \mathbf{e}'_{p_k}\right) + (1-c_j) \sum_{l \in S_{\mathrm{NC}}} w^{\star}_l \left(\mathbf{r}'_{p_l} + \mathbf{e}'_{p_l}\right), \quad j = 1, 2 \cdots K \tag{16}$$

where c_j denotes the fractional area of the cyan colorant corresponding to the digital value C_j; $\mathbf{r}^{\star\prime}_{c_j}$ is the reflectance of the multicolorant step-wedge print with cyan digital value C_j; the sets S_C and S_{NC} represent a partition of the primary indices $\{2, 3, \ldots 15\}$, such that the elements of S_C correspond to the primaries having the cyan colorant as a constituent and elements of S_{NC} correspond to the primaries that do not have the cyan colorant as a constituent; and

$$w^{\star}_k = \begin{cases} \dfrac{w^j_k}{c_j} & k \in S_C \\ \dfrac{w^j_k}{1-c_j} & k \in S_{\mathrm{NC}} \end{cases}$$

where w^j_k is the fractional area of the kth primary for the jth step print (as in (13)). Using (3), we can see that the factors $w^{\star}_k, w^{\star}_l \in \{(1-m)(1-y)(1-k), (1-m)(1-y)k, (1-m)y(1-k), (1-m)yk, m(1-y)(1-k), m(1-y)k, my(1-k), myk\}$, where m, y, and k are the (fixed) dot areas for the magenta, yellow, and black colorants for the whole multicolorant cyan step-wedge. Note that the factors $w^{\star}_k$ and $w^{\star}_l$ are constant over the entire step wedge and can be precomputed from the m, y, and k values, which are known from the single-colorant step-wedge estimation. These equations can be further rewritten as

$$(\mathbf{r}^{\star}_{\mathrm{pc}} + \mathbf{e}^{\star}_{\mathrm{pc}}) c_j = \mathbf{r}^{\star}_{\mathrm{cw}_j} + \mathbf{e}^{\star}_{\mathrm{cw}_j}, \quad j = 1, 2 \cdots K \tag{17}$$

where

$$\begin{aligned} \mathbf{r}^{\star}_{\mathrm{cw}_j} &= \mathbf{r}^{\star\prime}_{c_j} - \sum_{l \in S_{\mathrm{NC}}} w^{\star}_l \mathbf{r}'_{p_l}, \\ \mathbf{r}^{\star}_{\mathrm{pc}} &= \sum_{k \in S_C} w^{\star}_k \mathbf{r}'_{p_k} - \sum_{l \in S_{\mathrm{NC}}} w^{\star}_l \mathbf{r}'_{p_l} \end{aligned} \tag{18}$$

and $\mathbf{e}^{\star}_{\mathrm{pc}}$, $\mathbf{e}^{\star}_{\mathrm{cw}_j}$ are the corresponding combined errors. The K equations in (17) may be combined as

$$(\mathbf{r}^{\star}_{\mathrm{pc}} + \mathbf{e}^{\star}_{\mathrm{pc}}) \mathbf{c}^{\mathbf{T}} = \mathbf{R}^{\star}_{\mathrm{cw}} + \mathbf{E}^{\star}_{\mathrm{cw}} \tag{19}$$

where $\mathbf{R}^{\star}_{\mathrm{cw}} = [\mathbf{r}^{\star}_{\mathrm{cw}_1} \cdots \mathbf{r}^{\star}_{\mathrm{cw}_N}]$, and $\mathbf{E}^{\star}_{\mathrm{cw}} = [\mathbf{e}^{\star}_{\mathrm{cw}_1} \cdots \mathbf{e}^{\star}_{\mathrm{cw}_N}]$. If we further constrain the digital control values of cyan in the multicolorant step-wedge of cyan sweeps to be consistent with those in single-colorant cyan step-wedge, and combine single step-wedges (15) and multicolorant step-wedges (19), we get

$$\left(\begin{bmatrix} \mathbf{r}'_{\mathrm{pc}} \\ \mathbf{r}^{\star}_{\mathrm{pc}} \end{bmatrix} + \begin{bmatrix} \mathbf{e}'_{\mathrm{pc}} \\ \mathbf{e}^{\star}_{\mathrm{pc}} \end{bmatrix} \right) \mathbf{c}^{\mathbf{T}} = \begin{bmatrix} \mathbf{R}'_c \\ \mathbf{R}^{\star}_{\mathrm{cw}} \end{bmatrix} + \begin{bmatrix} \mathbf{E}'_c \\ \mathbf{E}^{\star}_{\mathrm{cw}} \end{bmatrix} \tag{20}$$

where the terms are the same as defined in (15) and (19). The dot growth function for the cyan colorant can now

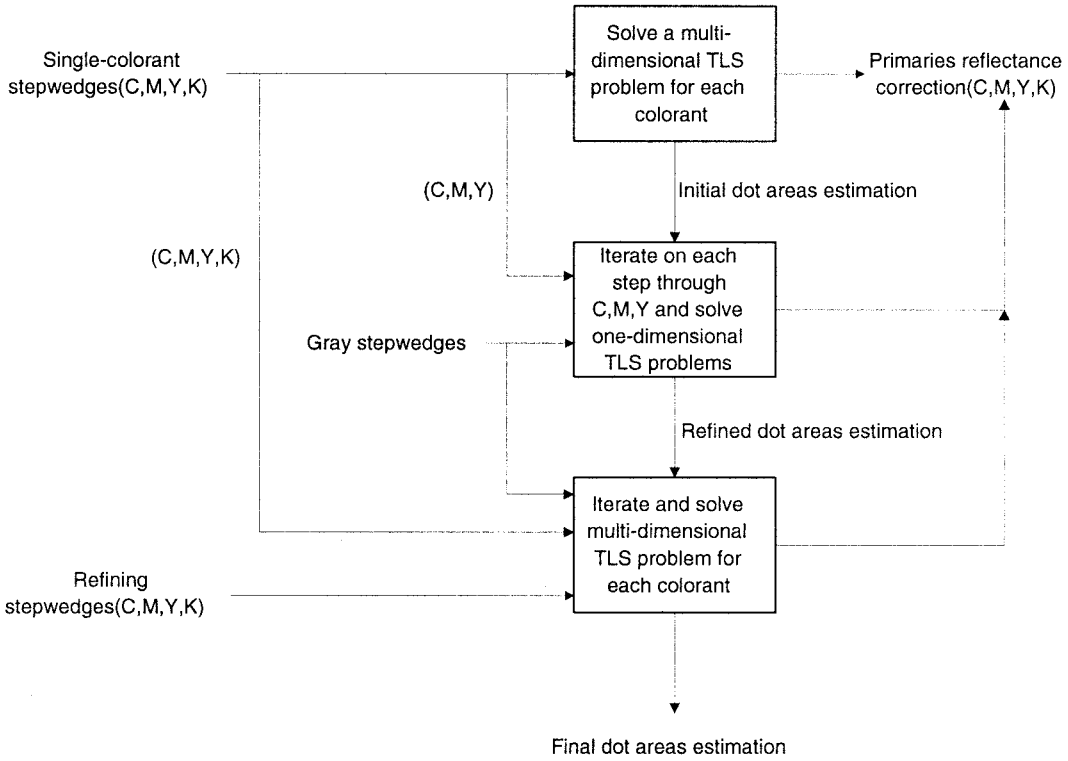

Fig. 5. Dot growth function estimation for random mixing model—TLS solution by employing single-colorant, gray, and multicolorant step-wedges.

be obtained by "solving" the above system of equations as a multidimensional TLS problem. Note that this procedure requires the knowledge of the dot growth functions of the other colorants and can therefore be used only as a refining step. The TLS solution also provides "corrections" $\mathbf{e}'_{\rm pc}$ and $\mathbf{e}^{\star}_{\rm pc}$ for the left hand side in (20). $\mathbf{e}^{\star}_{\rm pc}$ is not useful because it corresponds to the compound term, but $\mathbf{e}'_{\rm pc}$ can be used to get the "updated" cyan primary $(\mathbf{r}'_{\rm pc}+\mathbf{e}'_{\rm pc})$.

The above description focuses on the dot growth function estimation for the cyan colorant. The same approach can be applied to the other colorants, wherein the dot growth function for each colorant is estimated using TLS similar to (20), by keeping the dot areas of the other colorants fixed. This procedure can then be iteratively repeated for the four colorants until the error becomes sufficiently small.

2) Refinement Using Gray Step-Wedge: Although the gray step-wedge is a special case of multicolorant step-wedges, it is worthwhile to discuss it and incorporate it into the training samples, because the accurate rendering of gray tones is very important for a color printer [4]. Consider a K-step gray wedge with CMY digital values $\{C_j = M_j = Y_j\}_{j=1}^{K}$. We assume that initial estimates of the dot growth functions have been obtained from single-colorant step-wedges. The reflectance for the jth step of the gray wedge can be utilized to refine the cyan dot area estimate c_j. By following the same grouping process used in (16), we get

$$\mathbf{r}'_{g_j}+\mathbf{e}'_{g_j} = c_j \sum_{k\in S_C} w_k^{j\star}\left(\mathbf{r}'_{p_k}+\mathbf{e}'_{p_k}\right) + (1-c_j)\sum_{l\in S_{\rm NC}} w_l^{j\star}\left(\mathbf{r}'_{p_l}+\mathbf{e}'_{p_l}\right) \tag{21}$$

where $\mathbf{r}'_{g_j}$ denotes the reflectance for jth step of the gray wedge; S_C, $S_{\rm NC}$ are as defined earlier, and

$$w_k^{j\star} = \begin{cases} \dfrac{w_k^j}{c_j} & k\in S_C \\ \dfrac{w_k^j}{1-c_j} & k\in S_{\rm NC} \end{cases}$$

where w_k^j is the fractional area of the kth primary for the jth step print. Using the Demichel equation (3), we can see that the factors $w_k^{j\star}, w_l^{j\star} \in \{(1-m_j)(1-y_j)(1-k_j), (1-m_j)(1-y_j)k_j, (1-m_j)y_j(1-k_j), (1-m_j)y_jk_j, m_j(1-y_j)(1-k_j), m_j(1-y_j)k_j, m_jy_j(1-k_j), m_jy_jk_j\}$, where m_j, y_j, and k_j are the dot areas for the magenta, yellow, and black colorants on the jth step print of the gray wedge. Since, in this case, the factors $w_k^{j\star}$ and $w_l^{j\star}$ are not constant over the entire gray wedge, we can no longer combine the estimation of the cyan dot growth function into a single multidimensional TLS problem as was done in (20) for the multicolorant step-wedges. Nevertheless, we can refine the dot areas of the four colorants on each step individually. Combining the above equation with the corresponding single cyan step-wedge on step j (with equal digital value C_j, therefore equal colorant dot area c_j) in (14), we get

$$\left(\begin{bmatrix}\mathbf{r}'_{\rm pc}\\ \mathbf{r}^{\star}_{pg_j}\end{bmatrix}+\begin{bmatrix}\mathbf{e}'_{\rm pc}\\ \mathbf{e}^{\star}_{pg_j}\end{bmatrix}\right)c_j = \begin{bmatrix}\mathbf{r}'_{c_j}\\ \mathbf{r}^{\star}_{g_j}\end{bmatrix}+\begin{bmatrix}\mathbf{e}_{c_j}\\ \mathbf{e}^{\star}_{g_j}\end{bmatrix} \tag{22}$$

where

$$\mathbf{r}^{\star}_{g_j} = \mathbf{r}'_{g_j} - \sum_{l\in S_{\rm NC}} w_l^{j\star}\mathbf{r}'_{p_l},$$

$$\mathbf{r}^{\star}_{pg_j} = \sum_{k\in S_C} w_k^{j\star}\mathbf{r}'_{p_k} - \sum_{l\in S_{\rm NC}} w_l^{j\star}\mathbf{r}'_{p_l}$$

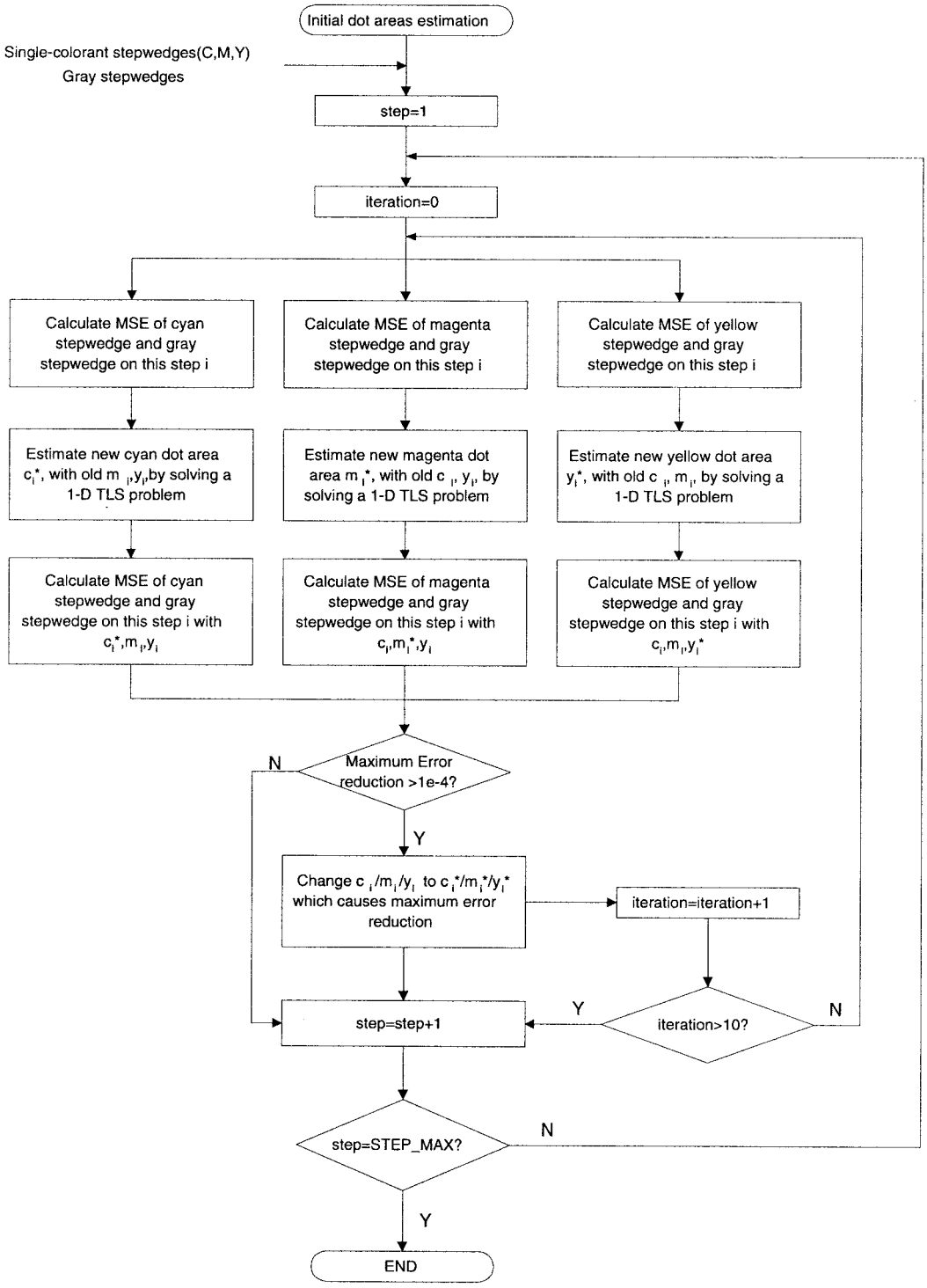

Fig. 6. Dot growth function estimation for random mixing model—TLS iteration on gray step-wedge.

and $\mathbf{e}^{\star}_{pg_j}$, $\mathbf{e}^{\star}_{g_j}$ are the corresponding combined errors. This equation may now be solved as a 1-D TLS problem to obtain the dot area c_j. The same procedure is repeated at each step, to refine the complete dot growth functions for cyan, and subsequently for the other colorants. Again, $\mathbf{e}^{\star}_{pg_i}$ is not useful because it corresponds to the compound error, but $\mathbf{e}'_{\mathrm{pc}}$ can be used to get the "updated" cyan primary $(\mathbf{r}'_{\mathrm{pc}} + \mathbf{e}'_{\mathrm{pc}})$.

3) Combination of All Step-Wedges: In practice, we can combine all the above techniques together (see Fig. 5 for a flowchart of the complete algorithm). First, the initial dot growth functions are estimated from the single-colorant step-wedges by solving a multidimensional TLS problem (15). Then the gray wedge is employed to refine the dot areas estimation of all four colorants, one step at a time, by solving the 1-D TLS problem (22). At each iteration, we change the dot area of the colorant which causes the largest mean square error (MSE) improvement and iterate among the four colorants (a flowchart of the process is shown in Fig. 6). Finally, if additional multicolorant step-wedges are provided, they are utilized to further refine the estimation of the dot growth

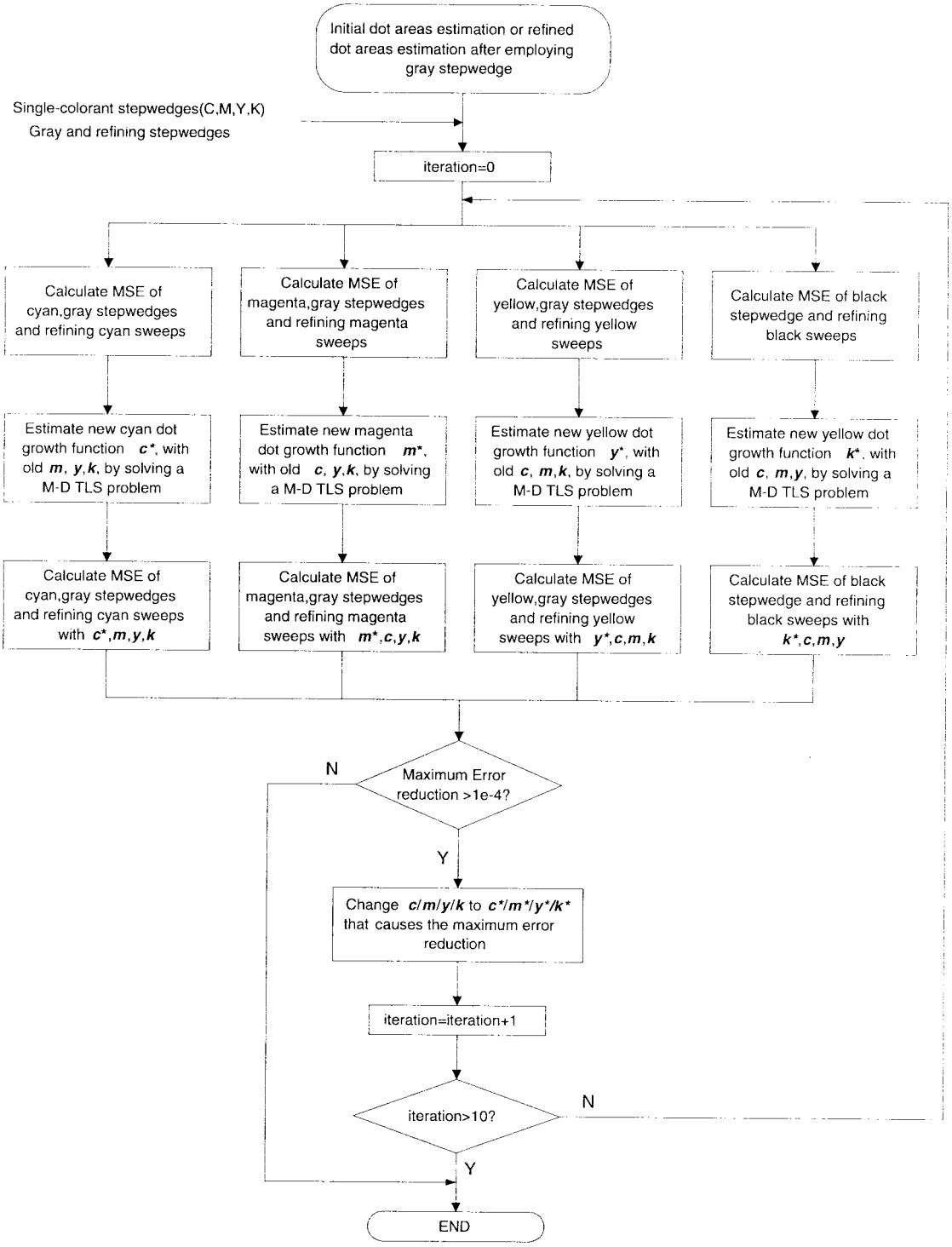

Fig. 7. Dot growth function estimation for random mixing model—TLS iteration on multicolorant step-wedges.

functions, by solving the multidimensional TLS problem (20). We iteratively refine the dot growth function of the colorant that causes the largest MSE improvement at each step as shown in Fig. 7. It should be noted that the primaries C, M, Y, and K will be "updated" after each estimation step.

D. TLS for the Dot-on-Dot Model with Selected Primary Updates

For the dot-on-dot model, multicolorant step-wedges can be used to refine the dot growth functions in a manner similar to the case of the random mixing model. However, since the number of effective primaries reduces to five (instead of 16) in a given region for a dot-on-dot screen printer, the details of the equations are different. Following the same notations in Section II-A2, we will let p_1, p_2, p_3, p_4 denote the printer colorants in increasing dot area order, and a_1, a_2, a_3, a_4 are the corresponding dot areas. Suppose we select one multicolorant step-wedge where only the digital value of colorant p_1 varies between zero and 255, while the digital values (and therefore

fractional areas) of the other three colorants remain constant, and let a_1^j denotes the dot area of colorant p_1 on step j, a_2, a_3, a_4 denote the dot areas of the other three colorants which are kept constant throughout this step-wedge (note that a_2, a_3, and a_4 have already been estimated from the single-colorant step-wedges), then from (4) and (13), we get

$$(\mathbf{r}'_{p_1p_2p_3p_4} - \mathbf{r}'_{p_2p_3p_4})a_1^j = \mathbf{r}' - a_2\mathbf{r}'_{p_2p_3p_4} - (a_3 - a_2)\mathbf{r}'_{p_3p_4} - (a_4 - a_3)\mathbf{r}'_{p_4}. \quad (23)$$

After incorporating the error terms, we can rewrite the equation as

$$(\mathbf{r}^\star_{pa_1} + \mathbf{e}^\star_{pa_1})a_1^j = \mathbf{r}^\star + \mathbf{e}^\star \quad (24)$$

where $\mathbf{r}^\star_{pa_1} = \mathbf{r}'_{p_1p_2p_3p_4} - \mathbf{r}'_{p_2p_3p_4}, \mathbf{r}^\star = \mathbf{r}' - a_2\mathbf{r}'_{p_2p_3p_4} - (a_3 - a_2)\mathbf{r}'_{p_3p_4} - (a_4 - a_3)\mathbf{r}'_{p_4}$, and $\mathbf{e}^\star_{pa_1}$, $\mathbf{e}^\star$ represent the corresponding combined errors.

Obviously, the above equations can be solved by using the method of TLS. Indeed, we can combine the multicolorant step-wedge equation (24) and single-colorant step-wedge equation (14) to form a single TLS problem. Thus, by solving the equation (suppose p_1 is cyan and therefore $a_1^j = c_j$)

$$\left(\begin{bmatrix}\mathbf{r}'_{\mathrm{pc}}\\ \mathbf{r}^\star_{pa_1}\end{bmatrix} + \begin{bmatrix}\mathbf{e}'_{\mathrm{pc}}\\ \mathbf{e}^\star_{pa_1}\end{bmatrix}\right)c_j = \begin{bmatrix}\mathbf{r}'_{c_j}\\ \mathbf{r}^\star\end{bmatrix} + \begin{bmatrix}\mathbf{e}'_{\mathrm{pc}}\\ \mathbf{e}^\star\end{bmatrix} \quad (25)$$

we can simultaneously refine the dot area of cyan on step j, and "update" the cyan primary (note that $\mathbf{e}^\star_{pa_1}$ is not useful since it corresponds to the compound term $\mathbf{r}^\star_{pa_1}$). For the gray step-wedge, a similar iteration can be carried out among the four colorants (see Section III-C2). However, if additional multicolorant step-wedges are provided, the dot areas on all steps for one colorant cannot be perturbed jointly by solving a multidimensional TLS problem as in (20). This is because the term $\mathbf{r}_{pa_1}$ will generally differ among the multicolorant step-wedge corresponding to one colorant sweeps, making it impossible to form one "parameter" matrix A for TLS. Therefore, there would be no significant mathematical advantages in utilizing multicolorant step-wedges besides gray step-wedge, which is utilized in our experiment.

E. TLS for the Combined Model

As mentioned in Section II-A2, a combined model incorporating both dot-on-dot and random mixing usually improves the accuracy of the Neugebauer model for a printer with dot-on-dot configuration. However, as introduced in (5), the noise factor α, makes the equations nonlinear in the dot areas of the primaries and therefore cannot be solved readily. Thus, we suggest a slight modification of the combined Neugebauer model (5), where the combination is done in the YN-corrected reflectance space as

$$r^{1/n}(\lambda) = (1 - \alpha)r_d^{1/n}(\lambda) + \alpha r_r^{1/n}(\lambda) \quad (26)$$

where all the symbols have the same meaning as in (5). Through this modification, the combined model becomes linear in the dot areas and the mixing factor α and can therefore be solved by TLS regression.

F. TLS for Further Primary Estimation

Ideally, both the dot area estimates and the correction to the primary reflectances should be obtained simultaneously using TLS. However, the primary reflectance corrections can only be achieved for four single colorant primaries: C, M, Y, and K. In utilizing multicolorant step-wedges, the compound error terms [see (20) and (22)] cannot be utilized to correct the individual primaries. Nevertheless, the TLS-based technique is expected to produce better estimates for the dot growth functions than its LS counterpart due to its accountability of errors in the primaries. On the other hand, further primary correction can be achieved based on the dot growth functions already estimated. Consider M multicolorant patches printed on paper, whose spectral reflectance can be estimated by weighted combination of the 16 Neugebauer primaries (for a four colorant digital halftone printer) by

$$\mathbf{W}_{M\times 16}\mathbf{R}_{\mathbf{P}_{16\times N}} = \mathbf{R}_{M\times N} \quad (27)$$

where $W(i,j)$ is the fractional area of the ith color patch corresponding to the jth primary, $R_P(i,j)$ is the YN corrected reflectance of the ith primary at wavelength λ_j, and $R(i,j)$ is the YN corrected reflectance of the ith color patch at λ_j. Alternatively, if the M multicolorant patches are measured directly, they can be viewed as M observations of linear combinations of the Neugebauer primaries. In fact, by solving (27) for $\mathbf{R_P}$, assuming $\mathbf{W}$ and $\mathbf{R}$ are known, we can directly estimate the primaries. $\mathbf{W}$ can be computed based on the already estimated dot growth functions, and $\mathbf{R}$ can be measured directly. It can be easily seen that the measurement of $\mathbf{R}$ is subject to error. So $\mathbf{R_P}$ can be predicted by solving an LS problem [21]:

$$\mathbf{W}\mathbf{R_P} = (\mathbf{R} + \Delta\mathbf{R}). \quad (28)$$

This approach, however, fails to account for errors in $\mathbf{W}$ arising due to estimation errors in the previous determined dot growth functions (from which $\mathbf{W}$ is computed). Therefore, it is more appropriate to estimate $\mathbf{R_P}$ by solving (27) in a TLS sense. Indeed, suppose $\Delta\mathbf{W}$ is the error contained in $\mathbf{W}$ and $\Delta\mathbf{R}$ is the error contained in $\mathbf{R}$, the TLS problem is

$$(\mathbf{W} + \Delta\mathbf{W})\mathbf{R_P} = (\mathbf{R} + \Delta\mathbf{R}). \quad (29)$$

Note that the multicolorant patches constituting $\mathbf{R}$ in the above approach can be arbitrary, unlike the multicolorant step-wedges employed in Section III-C1, which need to be sweeps of one colorant at a time while the other three colorants are held constant. In order to estimate $\mathbf{R_P}$ accurately, $\mathbf{R}$ should adequately represent the color spectra reproducible on the given device. This idea of further primary estimation can be applied to both the rotated screen printer (by random mixing model) and the dot-on-dot screen printer (by dot-on-dot model). If the combined model is used, the noise factor can be included in $\mathbf{W}$.

G. The Application of TLS Methods to Other Neugebauer Models

The TLS methods proposed in this paper can be extended to other Neugebauer models. For instance, consider the cellular

Neugebauer model where the printer's CMYK color space is divided into several "cells" and "partial dot area" primaries are introduced to enhance the modeling accuracy (see [27] for a detail description of the cellular Neugebauer model). The TLS methods can be applied to each cell to simultaneously estimate the dot growth functions and the correction to the partial dot area primaries. The same single-colorant and gray step-wedges can be utilized in the training chart as before. However, due to the same reason stated in Section III-C and Section III-F, only the primaries along the four single colorant C, M, Y, and K axes can be updated by TLS correction. If estimation of more primaries is desired, the technique mentioned in Section III-F can be employed, and more multicolorant patches should be printed in the training chart to ensure enough sampling of the color space.

IV. Results

In order to test the efficiency and accuracy of the TLS techniques, several experiments were carried out on two halftone printers: A and B. Both printers use four colorants (C, M, Y, K) with independent halftone screens. Printer A uses a rotated line screen that approximates the random mixing assumption and printer B employs a dot-on-dot screen which is representative of the dot-on-dot model. In each case, the TLS based algorithm is compared with its LS counterpart.

A training chart with four sets of single- and multicolorant step-wedges, and a gray step-wedge is used to compute the model parameters. Each single-colorant step-wedge has 17 steps evenly distributed between zero and 255 (zero and 255 included). The gray step-wedge also has 17 steps along the $(C = M = Y)$ line. The multicolorant step-wedges have one colorant varying from zero to 255 at digital values identical to the single-colorant step-wedges, while the other three colorants are kept fixed at a constant level.

An independent test chart with 125 samples was utilized to test the various proposed algorithms. The chart was generated by sampling the device CMY space on a uniform 5 $\times$ 5 $\times$ 5 grid. A default undercolor removal [4] algorithm was employed to convert from CMY to CMYK. The spectral reflectances of the step-wedges in the training and test chart were measured over a 400 to 700 nm range with a 10 nm sampling interval using a Gretag spectrophotometer. The measurements from the training chart were used to estimate the dot growth functions for the C, M, Y, K colorants, the YN parameter n, and the noise factor α. These model parameters were then used to obtain reflectance predictions for the CMYK digital values corresponding to the patches on the test chart. Both the measured and the predicted reflectances were converted to CIELAB color values [2] under the CIE viewing Illuminant D50. Color differences between the measurements and the predictions were then computed using three common color difference metrics: $\Delta E^{\star}_{ab}$ [2], $\Delta E^{\star}_{\mathrm{CMC}}$ [28], and $\Delta E^{\star}_{94}$ [29].

A. Random Mixing Model

For printer A, which employs rotated screens, the random mixing Neugebauer model is used. Six techniques for estimating the dot area functions and the YN correction factor n were tested as follows:

1) LS estimation, employing single-colorant step-wedges;
2) TLS estimation, employing single-colorant step-wedges;
3) LS estimation, employing single-colorant and gray step-wedges;
4) TLS estimation, employing single-colorant and gray step-wedges;
5) LS estimation, employing single-colorant, gray and multicolorant step-wedges;
6) TLS estimation, employing single-colorant, gray and multicolorant step-wedges.

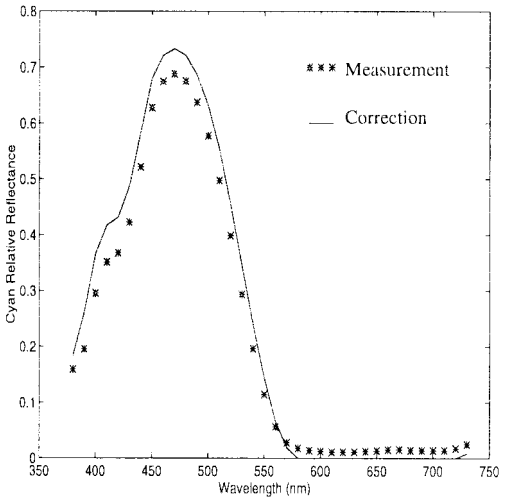

Fig. 8. Primary cyan reflectance curve correction in TLS estimation (employing single-colorant step-wedges; YN correction factor $n = 2.0$).

Correction of the primary reflectance curves for the single colorant primaries R_C, R_M, R_Y, R_K is performed in Techniques 2, 4, and 6. An example of the cyan primary (R_c) correction is shown in Fig. 8. Since the motivation for the TLS technique was to account for measurement errors in the primary reflectances, it is useful to compare the primary correction to estimates in measurement error for the Gretag spectrophotometer. These measurement errors were estimated by utilizing a color chart specifically designed for that purpose. The color chart encompasses: 1) Fifty patches for each colorant (C, M, Y, K) where each patch contains 50% (i.e., a digital value of 128) of the colorant, and 2) Fifty intermediate gray patches with digital values of $C = M = Y = 128$. The chart was printed ten times on Printer A. The spectral reflectance for all color patches were then measured using the spectrophotometer. From these measurements, the mean, the standard deviation, and the maximum deviation from the mean for the cyan, magenta, yellow, black, and gray were computed. The overall standard deviation and maximum measurement error were also estimated by averaging among the individual ones. The results are shown in Fig. 9. The difference between the measured and the TLS corrected cyan primary in Fig. 8 is also shown in Fig. 9. Note that the difference at some points exceeds the maximum measurement error and the "3σ" threshold (where σ is the overall standard deviation). This difference can probably be attributed to the intrinsic "model

σ	0.0088
3σ	0.0264
max error	0.0271

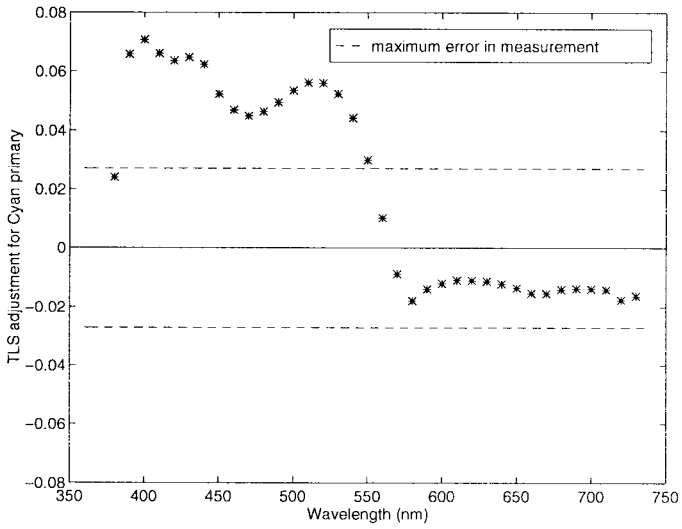

Fig. 9. Difference between cyan primary measurement and the TLS correction in Fig. 8 (σ—the overall standard deviation of measurement error; max error—the overall maximum measurement error).

TABLE I

AVERAGE, MAXIMUM, AND STANDARD DEVIATION OF ΔE ERRORS IN PREDICTING THE TEST CHART (WITH YN CORRECTION FACTOR n AND α OPTIMIZED). (1) LS (LS_G) AND TLS (TLS_G) REGRESSION FOR THE PRINTER WITH ROTATED SCREEN (RANDOM MIXING MODEL APPLIED), EMPLOYING SINGLE-COLORANT AND GRAY STEP-WEDGES; (2) LS (LS_GM) AND TLS (TLS_GM) FOR THE ROTATED SCREEN PRINTER, EMPLOYING SINGLE-COLORANT, GRAY AND MULTICOLORANT STEP-WEDGES; (3) LS (LS_GD) AND TLS (TLS_GD) FOR THE DOT-ON-DOT SCREEN PRINTER (COMBINED MODEL APPLIED), EMPLOYING SINGLE-COLORANT AND GRAY STEP-WEDGES

LS and TLS estimation results (test chart prediction error)							
ΔE		Rotated screen				Dot-on-dot screen	
		LS_G (n=6.5)	TLS_G (n=5.5)	LS_GM (n=6.5)	TLS_GM (n=5.5)	LS_GD (n=8.0;α=0.5)	TLS_GD (n=8.0;α=0.5)
$\Delta E^{\star}_{ab}$	Avg	6.14	6.00	5.40	5.34	4.46	4.41
	Max	13.14	12.02	11.81	11.58	11.46	10.91
	σ	2.36	2.30	2.30	2.28	2.19	2.01
$\Delta E^{\star}_{CMC}$	Avg	4.06	3.97	3.64	3.53	2.70	2.65
	Max	11.27	10.55	10.41	10.03	6.24	5.67
	σ	2.14	2.03	2.01	1.95	1.32	1.19
$\Delta E^{\star}_{94}$	Avg	3.05	2.97	2.95	2.91	2.87	2.83
	Max	7.02	6.78	6.63	6.29	5.14	4.91
	σ	2.71	2.57	2.39	2.28	1.35	1.22

error" in the Neugebauer model, which is an approximation of the complicated physical printing process.

Fig. 10 shows the average $\Delta E^{\star}_{ab}$, $\Delta E^{\star}_{\mathrm{CMC}}$, and $\Delta E^{\star}_{94}$ errors between the measured $L^{\star}a^{\star}b^{\star}$ values for the single-colorant step-wedges (found within the training chart) and their corresponding model predictions obtained by utilizing the LS and TLS based techniques respectively. It can be seen that the TLS based technique produces smaller ΔE errors in all three cases than its LS counterpart. In addition, Fig. 12 shows the average $\Delta E^{\star}_{ab}$, $\Delta E^{\star}_{\mathrm{CMC}}$, and $\Delta E^{\star}_{94}$ errors between the measured $L^{\star}a^{\star}b^{\star}$ values of the test chart and their corresponding model predictions obtained by utilizing Techniques 1–6. Similarly, the predictions obtained by the TLS based techniques are more accurate than their LS counterparts. Note that the gray and multicolorant step-wedges add significant improvements, regardless of the technique employed (LS or TLS), since the dot area functions generally vary with the overlap of multiple colorant dots. Therefore, the utilization of the gray and multicolorant step-wedges compensates for this effect.

Table I shows the smallest ΔE errors (average, maximum and standard deviation for the test chart) achieved by Techniques 3, 4, 5, and 6, with YN correction factor n optimized in each case. Again, the TLS techniques consistently outperformed their LS counterparts. Though the improvement of TLS over LS decreases as more step-wedges were employed, the TLS method is consistently better than LS and the improvement in maximum ΔE errors is still significant. Also note that when only a limited number of print samples are available due to limitations of measurement time, the TLS method offers significant improvement over the LS method.

B. Dot-on-Dot Model

For printer B, which employs a dot-on-dot screen, the dot-on-dot and the combined models of Section III-E are used. The following four techniques for estimating the dot area functions, and the YN correction factor were tested:

1) LS estimation, employing single-colorant step-wedges (pure dot-on-dot model);

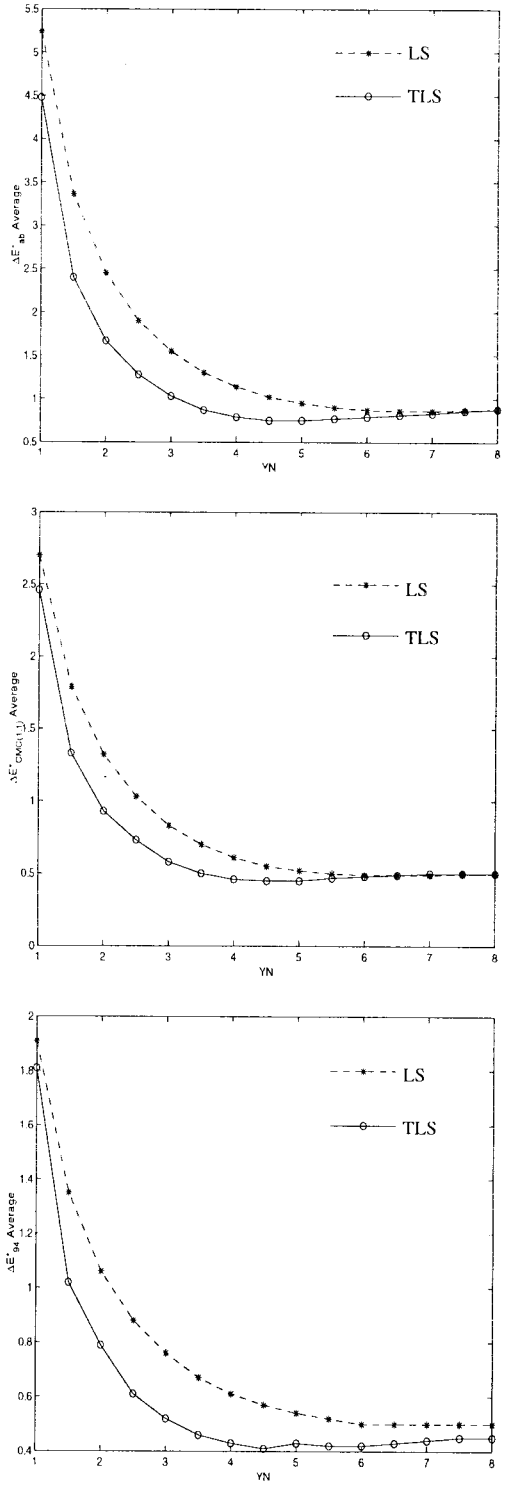

Fig. 10. LS and TLS average ΔE errors for the single-colorant training set patches using Printer A (random mixing model applied).

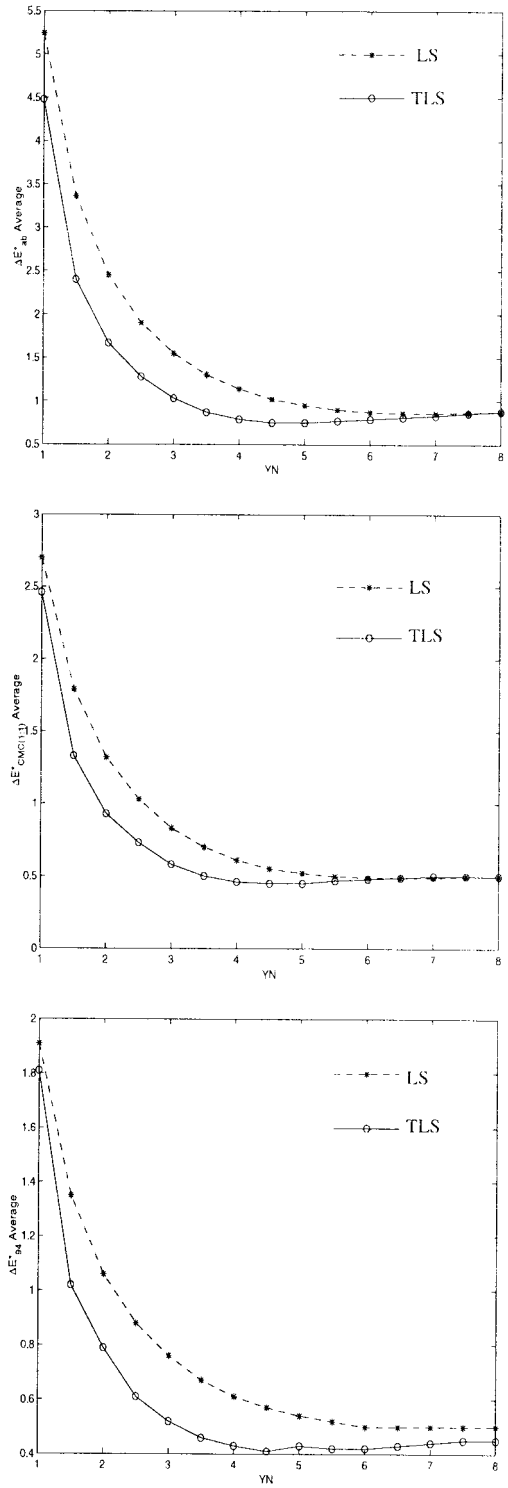

Fig. 11. LS and TLS average ΔE errors for the single-colorant training set patches using Printer B (dot-on-dot model applied).

2) TLS estimation, employing single-colorant step-wedges (pure dot-on-dot model);
3) LS estimation, employing single-colorant and gray step-wedges (combined model);
4) TLS estimation, employing single-colorant and gray step-wedges (combined model).

Techniques 1 and 2 use the pure dot-on-dot model (3) since the dot-on-dot and random mixing models are identical over single colorant patches; and the noise factor α cannot be estimated unless multicolorant patches are used in the estimation. Since the printing process is subject to misregistration errors, the pure dot-on-dot model that assumes no noise and perfect registration is not appropriate. This was apparent in our experiments, where the inclusion of gray step-wedges provided little improvement for the pure dot-on-dot Neugebauer model. The results for this case are therefore not included here.

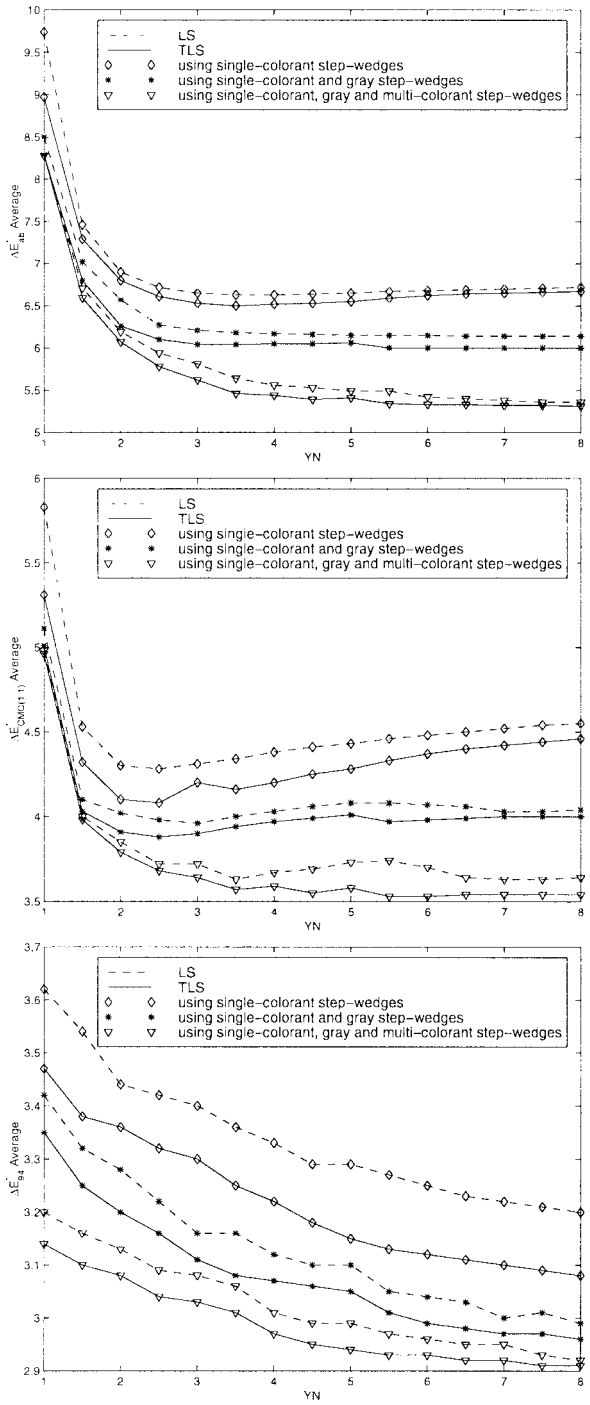

Fig. 12. Average ΔE errors for the test chart for Printer A (random mixing model applied). (1) LS and TLS estimation, employing single-colorant step-wedges; (2) LS and TLS estimation, employing single-colorant and gray step-wedges; (3) LS and TLS estimation, employing single-colorant, gray and multicolorant step-wedges.

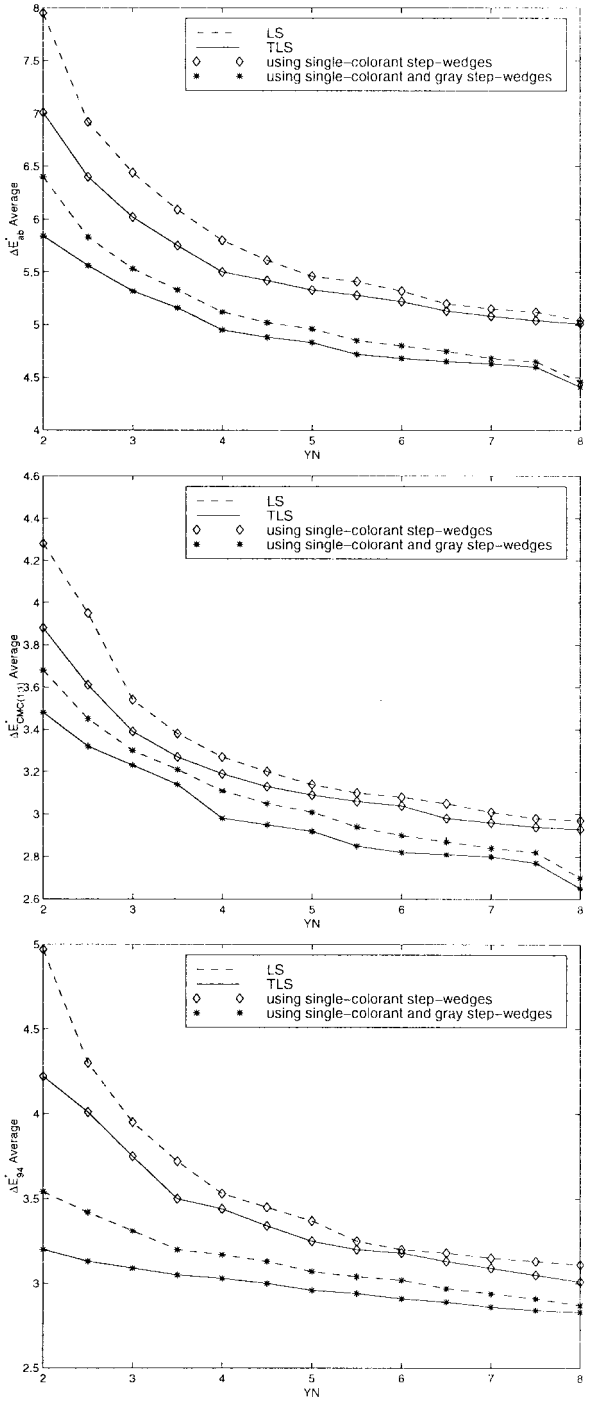

Fig. 13. Average ΔE errors for the test chart for Printer B (dot-on-dot model applied). (1) LS and TLS estimation, employing single-colorant step-wedges; (2) LS and TLS estimation, utilizing combined model ($\alpha = 0.5$), employing single-colorant and gray step-wedges.

The combined Neugebauer model (26) was hence used for Techniques 3 and 4, which utilize gray step-wedges in addition to the single-colorant prints.

Fig. 11 shows the average $\Delta E^{\star}_{ab}$, $\Delta E^{\star}_{\mathrm{CMC}}$, and $\Delta E^{\star}_{94}$ errors between the measured $L^{\star}a^{\star}b^{\star}$ values for the single-colorant step-wedges (found within the training chart) and their corresponding model predictions obtained by utilizing the LS and TLS based techniques respectively. In addition, Fig. 13 shows the same color difference metrics for the test chart patches using Techniques 1–4. Table I shows the smallest ΔE errors (average, maximum and standard deviation for the test chart) achieved by Techniques 3 and 4 with YN correction factor n and the noise factor α optimized in each case. Similar to the random mixing model, the predictions obtained by the TLS-based techniques are more accurate than their LS counterparts. Note that the gray step-wedge and the combined Neugebauer model add significant improvements, as can be

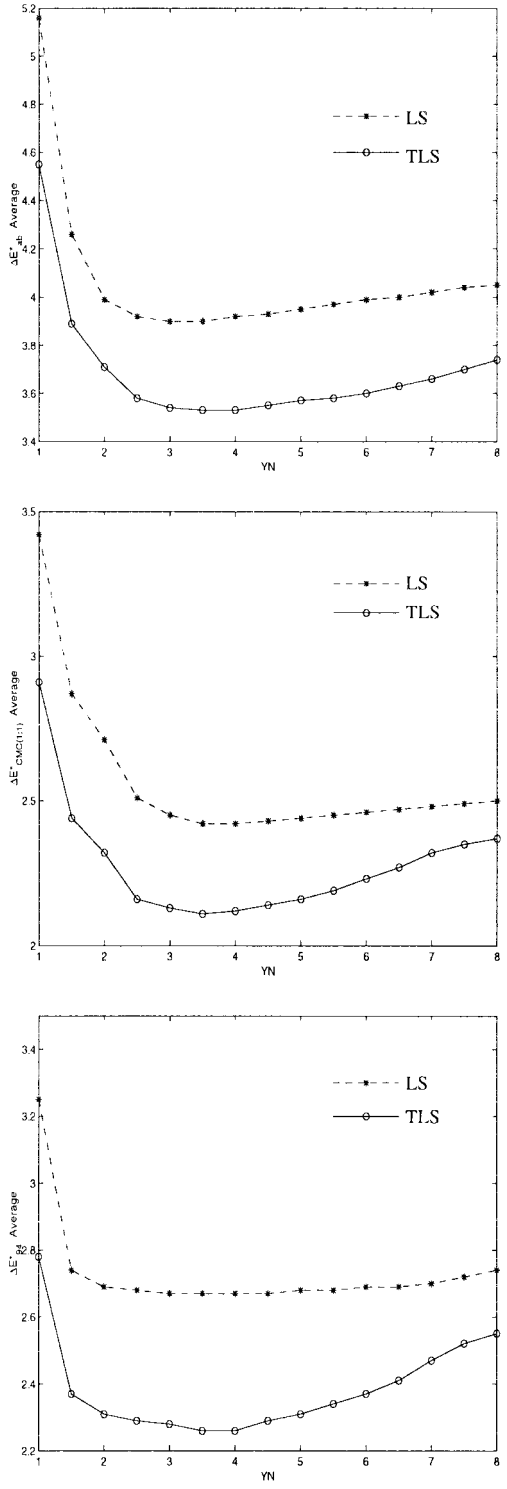

Fig. 14. Average ΔE errors for the test chart for Printer A (random mixing model applied) after further primary correction (using multicolorant samples $6 \times 6 \times 6$—LS and TLS regression, employing single-colorant step-wedges for the dot growth function estimation.

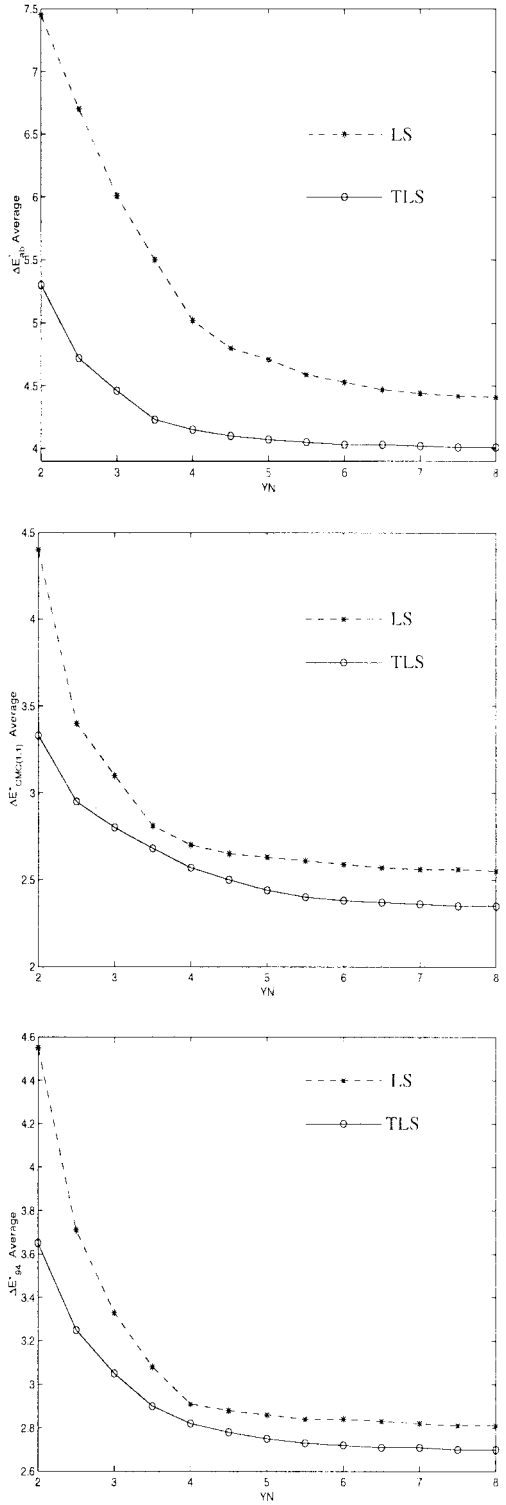

Fig. 15. Average ΔE errors for the test chart for Printer B (dot-on-dot mixing model applied) after further primary correction (using multicolorant samples $6 \times 6 \times 6$—LS and TLS regression, employing single-colorant step-wedges for the dot growth function estimation.

seen from Fig. 13, regardless of the technique employed (LS or TLS).

C. Further Primary Estimation

After estimating the dot growth functions, further primary estimation was performed by printing and measuring additional multicolorant patches. Indeed, $6 \times 6 \times 6$ patches were sampled uniformly in CMY color space, and undercolor removal/gray component replacement [4] was performed afterwards to convert from CMY to CMYK values. The same 125 test patches as in Sections IV-A and IV-B were printed and measured to test the performance of the different algorithms.

TABLE II
AVERAGE, MAXIMUM, AND STANDARDDEVIATION OF ΔE ERRORS IN PREDICTING THE TEST CHART (WITH n AND α OPTIMIZED) AFTER DOT GROWTH FUNCTION ESTIMATION AND FURTHER PRIMARY CORRECTION (WITH MULTICOLORANT SAMPLES $6 \times 6 \times 6$). (1) LS (LS_G_FC) AND TLS (TLS_G_FC) REGRESSION FOR THE ROTATED SCREEN PRINTER, EMPLOYING SINGLE-COLORANT AND GRAY STEP-WEDGES FOR THE DOT GROWTH FUNCTION ESTIMATION; (2) LS (LS_GM_FC) AND TLS (TLS_GM_FC) FOR THE ROTATED SCREEN PRINTER, EMPLOYING SINGLE-COLORANT, GRAY AND MULTICOLORANT STEP-WEDGES FOR THE DOT GROWTH FUNCTION ESTIMATION; (3) LS (LS_GD_FC) AND TLS (TLS_GD_FC) FOR THE DOT-ON-DOT SCREEN PRINTER, EMPLOYING SINGLE-COLORANT AND GRAY STEP-WEDGES FOR THE DOT GROWTH FUNCTION ESTIMATION

LS and TLS estimation with further primary correction (test chart prediction error)							
$\Delta \mathbf{E}$		Rotated screen				Dot-on-dot screen	
		LS_G_FC (n=3.0)	TLS_G_FC (n=3.5)	LS_GM_FC (n=3.0)	TLS_GM_FC (n=3.5)	LS_GD_FC (n=8.0;α=0.3)	TLS_GD_FC (n=8.0;α=0.1)
$\Delta E^{\star}_{ab}$	Avg	3.90	3.53	3.49	3.25	4.39	4.19
	Max	8.05	7.27	7.42	7.04	9.35	8.77
	σ	1.70	1.56	1.51	1.37	1.90	1.68
$\Delta E^{\star}_{CMC}$	Avg	2.42	2.11	2.05	1.89	2.55	2.45
	Max	5.15	4.33	4.42	4.11	5.01	4.86
	σ	1.04	0.85	0.78	0.69	1.02	0.94
$\Delta E^{\star}_{94}$	Avg	2.67	2.26	2.21	2.04	2.81	2.70
	Max	4.68	4.14	4.22	3.98	4.61	4.48
	σ	1.08	0.92	0.84	0.76	1.14	0.99

Both the LS and TLS based primary estimation were tested on printer A and B. Again, $\Delta E^{\star}_{ab}$, $\Delta E^{\star}_{\mathrm{CMC}}$, and $\Delta E^{\star}_{94}$ errors between the measurement and the model prediction were calculated. These are shown in Figs. 14 and 15. Note that the dot area function estimations were performed by employing only single-colorant step-wedges for both the LS and TLS based techniques. The TLS technique results in a better prediction than its LS counterpart, since it allows for errors in both the reflectance measurements $\mathbf{R}$ and the fractional area matrix $\mathbf{W}$.

It is also possible to perform further primary estimation after employing single-colorant, gray and/or multicolorant step-wedges to estimate the dot area functions. These results are shown in Table II with the optimum YN correction factor n and the noise factor α (for the combined dot-on-dot model). Again, the TLS-based results produce smaller ΔE errors than their LS counterparts. Comparing Table II with Table I, where TLS primary correction was performed on only four primaries, it is clear that further primary correction improves the accuracy of the Neugebauer model predictions.

V. CONCLUSION

This paper addresses the use of spectral Neugebauer models to characterize color halftone printers. The model parameters are determined from a few selective prints by utilizing total least square (TLS) based algorithms. The TLS algorithms are proposed due to their ability to provide a more suitable physical model than the least squares (LS) based techniques. These algorithms are applied on two common classes of color printers: 1) those utilizing conventional rotated screens for the color separations, and 2) those employing dot-on-dot halftone configurations. To this effect, they are tested on two representative printers and compared to their LS counterparts using several perceptually relevant color difference metrics. The results indicate that the TLS based approaches provide consistent and noticeable improvements over the LS based ones in printer characterization accuracy.

ACKNOWLEDGMENT

The authors wish to thank the Invention Opportunity Program Committee and the Production Controller Software Development Team of Xerox Corporation for sponsoring this research and providing the appropriate facilities. In addition, we wish to thank Dr. R. Balasubramanian, J. E. Stinehour, and the reviewers for their helpful suggestions.

REFERENCES

[1] G. Sharma and H. J. Trussell, "Digital color imaging," *IEEE Trans. Image Processing*, vol. 6, pp. 901–932, July 1997.
[2] CIE, "Colorimetry," CIE Publication no. 15.2, Central Bureau of the CIE, Vienna, Austria, 1986.
[3] D. L. MacAdam, Ed., *Selected Papers on Colorimetry-Fundamentals*. Bellingham, WA: SPIE Optical Engineering Press, 1993.
[4] R. W. G. Hunt, *Measuring Color*, 2nd Ed. New York: Ellis Horwood, 1991.
[5] G. Wyszecki and W. S. Stiles, *Color Science: Concepts and Methods, Quantitative Data and Formulae*, 2nd Ed. New York: Wiley, 1982.
[6] G. Sharma, M. J. Vrhel, and H. J. Trussell, "Color imaging for multimedia," in *Proc. IEEE*, vol. 86, pp. 1088–1108, June 1998.
[7] P. C. Hung, "Colorimetric calibration in electronic imaging devices using a look-up table model and interpolations," *J. Electron. Imag.*, vol. 2, pp. 53–61, Jan. 1993.
[8] J. Z. Chang, C. A. Bouman, and J. P. Allebach, "Recent results in color calibration using sequential linear interpolation," in *Proc. IS&T's 47th Ann. Conf., ICPS'94: The Physics and Chemistry of Imaging Systems*, May 1994, vol. 2, pp. 500–505.
[9] R. Eschbach, Ed., *Recent Progress in Digital Halftoning*. IS&T, Springfield, VA, 1995.
[10] R. Ulichney, *Digital Halftoning*. Cambridge, MA: MIT Press, 1987.
[11] K. T. Knox, "Introduction to digital halftones," in *Proc. IS&T's 47th Ann. Conf., ICPS'94: The Physics and Chemistry of Imaging Systems*, May 1994, vol. 2, pp. 456–459.
[12] T. N. Pappas, C. K. Dong, and D. L. Neuhoff, "Measurement of printer parameters for model-based halftoning," *J. Electron. Imag.*, vol. 2, pp. 193–204, July 1993.
[13] K. Knox, C. Hains, and G. Sharma, "Automatic calibration of halftones," in *Proc. SPIE: Human Vision and Electronic Imaging*, B. E. Rogowitz and J. P. Allebach, Eds., 1996, vol. 2657, pp. 432–436.
[14] S. G. Wang, "Algorithm-independent color calibration for digital halftoning," in *Proc. IS&T/SID Fourth Color Imaging Conf.*, Nov. 1996, pp. 75–77.
[15] C. J. Rosenberg, "Measurement-based evaluation of a printer dot model for halftone algorithm tone correction," *J. Electron. Imag.*, vol. 2, pp. 205–212, July 1993.
[16] H. E. J. Neugebauer, "Die theoretischen Grundlagen des Mehrfarbenbuchdrucks," *Zeitschrift für Wissenschaftliche Photographie Photo-*

physik und Photochemie, vol. 36, pp. 73–89, Apr. 1937, reprinted in [22, pp. 194–202].
[17] J. A. C. Yule and W. J. Nielsen, "The penetration of light into paper and its effect on halftone reproduction," in *TAGA Proc.*, May 1951, pp. 65–76.
[18] F. R. Clapper and J. A. C. Yule, "Reproduction of color with halftone images," in *Proc. 7th Ann. Tech. Mtg. TAGA*, May 1955, pp. 1–14.
[19] J. A. S. Viggiano, "Modeling the color of multi-colored halftones," in *TAGA Proc.*, 1990, pp. 44–62.
[20] R. Balasubramanian, "Colorimetric modeling of binary color printers," in *Proc. IEEE Int. Conf. Image Processing*, Nov. 1995, vol. II, pp. 327–330.
[21] ——, "The use of spectral regression in modeling halftone color printers," in *Proc. IS&T/OSA Optics and Imaging in the Information Age*, Rochester, NY, Oct. 20–24, 1996, pp. 372–375.
[22] K. Sayangi, Ed., *Proc. SPIE: Neugebauer Memorial Seminar on Color Reproduction*, SPIE, Bellingham, WA, Dec. 1989, vol. 1184.
[23] R. Balasubramanian, "A printer model for dot-on-dot halftone screens," in *Proc. SPIE: Color Hard Copy and Graphic Arts IV*, 1995, vol. 2413, pp. 356–364.
[24] E. Demichel, in *Procédé*, 1924, vol. 26, pp. 17–21, 26–27.
[25] G. H. Golub and C. F. Van Loan, *Matrix Computations*, 2nd Ed. Baltimore, MD: The Johns Hopkins Univ. Press, 1989.
[26] S. Van Huffel and J. Vandewalle, *The Total Least Squares Problem: Computational Aspects and Analysis*, Society for Industrial and Applied Mathematics, Philadelphia, 1991.
[27] R. Rolleston and R. Balasubramanian, "Accuracy of various types of Neugebauer models," in *Proc. IS&T/SID Color Imaging Conf.: Transforms and Portability of Color*, Nov. 1993, vol. II, pp. 32–37.
[28] F. J. J. Clarke, R. McDonald, and B. Rigg, "Modification to the JPC79 color-difference formula," *J. Soc. Dyers Colorists*, vol. 100, pp. 128–132, 1984.
[29] CIE, "Industrial color difference evaluation," CIE Pub. 116-1995, Central Bureau of the CIE, Vienna, Austria, 1995.

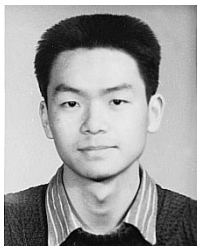

Minghui Xia received the B.S. degree in electronic engineering from Tsinghua University, Beijing, China in 1996, and M.S. degree in electrical engineering from University of Rochester, Rochester, NY, in May, 1998. He is currently a Ph.D. candidate in the Electrical Engineering Department, Princeton University, Princeton, NJ.

Eli Saber (S'91–M'96) received the A.S. degree in engineering science from the Mohawk Valley Community College, Utica, NY, in 1986, the B.S. degree in electrical and computer engineering from the State University of New York at Buffalo in 1988, and the M.S. and Ph.D. degrees in electrical and computer engineering (all with the highest honors) from the University of Rochester, Rochester, NY, in 1992 and 1996, respectively.

He joined the Supplies Development and Manufacturing Unit at The Document Company, Xerox, Webster, NY, in June 1988 as an Electrical, Instrumentation and Control Engineer involved in the design and development of toner production facilities. In June 1993, he was assigned to the Digital Imaging Technology Center, where he was involved in the design and development of image analysis, segmentation, annotation, and pattern recognition algorithms. In January 1995, he became a Research Assistant in the Department of Electrical Engineering, University of Rochester, and a Research and Development Engineer at Xerox, where he focused on the development of image/video processing algorithms targeted to search and analyze digital libraries. In January 1996, he joined the Products and Systems Group as a Research and Development Scientist, where he led the design and development of adaptive content dependent color image characterization/rendering algorithms and image quality specifications for internal color front ends destined to drive high quality/high speed print engines. In February 1997, he joined the Print Cartridge Delivery Unit as a Research and Development Scientist and Manager, where he is leading the characterization, both experimentally and theoretically, of the critical modules and components within black and white and color print engines. He is currently an Adjunct Faculty Member in the Electrical Engineering Department of both the University of Rochester and the Rochester Institute of Technology. His research interests include color image processing, color characterization, image/video segmentation, annotation, and indexing, and xerography.

Dr. Saber was the recipient of the Gibran Khalil Gibran Scholarship, and several prizes and awards for outstanding academic achievements from 1984 to 1988, as well as the Quality Recognition Award in 1990 from Xerox for his work in the design and engineering of toner productions facilities. He is also the recipient of several awards from Xerox Corporation for his work on the design and development of color front ends. He is a member of the Electrical Engineering Honor Society, Eta Kappa Nu, and the Imaging Science and Technology Society. He has a number of conference and journal publications. He is also a reviewer on the IEEE TRANSACTIONS ON IMAGE PROCESSING, the IEEE TRANSACTIONS ON PATTERN ANALYSIS AND MACHINE INTELLIGENCE, *Graphical Models and Image Processing Journal*, and the *Journal of Electronic Imaging*.

Gaurav Sharma (M'88) was born in Dehradun, India, on October 12, 1968. He received the B.E. degree in electronics and communication engineering from University of Roorkee, India in 1990, the M.E. degree in electrical communication engineering from the Indian Institute of Science, Bangalore, India, in 1992, and the M.S. degree in applied mathematics and Ph.D. degree in electrical engineering from North Carolina State University (NCSU), Raleigh, in 1995 and 1996, respectively.

From August 1992 through August 1996, he was a Research Assistant at the Center for Advanced Computing and Communications, Electrical and Computer Engineering Department, NCSU. Since August 1996, he has been a Member of Research and Technical Staff at the Digital Imaging Technology Center, Xerox Corporation, Webster, NY. His current research interests include color science and imaging, signal restoration, image halftoning, and error correction coding.

Dr. Sharma is a member of Sigma Xi, Phi Kappa Phi, the Society for Imaging Science and Technology, the IEEE Signal Processing Society, and the American Society for Engineering Education.

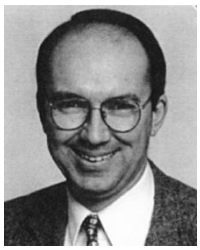

A. Murat Tekalp (S'80–M'82–SM'91) received M.S. and Ph.D. degrees in electrical, computer, and systems engineering from Rensselaer Polytechnic Institute (RPI), Troy, NY, in 1982 and 1984, respectively.

From December 1984 to August 1987, he was a senior research scientist at Eastman Kodak Company, Rochester, NY. In 1987, he became an Assistant Professor in the Electrical Engineering Department, University of Rochester, NY, where he is currently a Professor (http://www.ece.rochester.edu/~tekalp). His current research interests are in the area of digital image and video processing, including object-based video representations, motion tracking, image segmentation, image restoration, and multimedia content description.

Dr. Tekalp received the NSF Research Initiation Award in 1988, and named as Distinguished Lecturer by IEEE Signal Processing Society, in 1998. He has chaired the IEEE Signal Processing Society Technical Committee on Image and Multidimensional Signal Processing (January 1996 to December 1997). He has also served as an Associate Editor for the IEEE TRANSACTIONS ON SIGNAL PROCESSING (1990–1992), and IEEE TRANSACTIONS ON IMAGE PROCESSING (1994–1996). He is currently an Associate Editor for *Multidimensional Systems and Signal Processing*. He is also on the editorial boards of *Graphical Models and Image Processing* and *Visual Communication and Image Representation*, and the EURASIP journal, *Image Communication*. He is the author of *Digital Video Processing* (Englewood Cliffs, NJ: Prentice-Hall, 1995). He was appointed Technical Program Chair for the 1991 IEEE Signal Processing Society Workshop on Image and Multidimensional Signal Processing, and the Special Sessions Chair for the 1995 IEEE International Conference on Image Processing. He is the founder and first Chairman of the Rochester Chapter of the IEEE Signal Processing Society. He also served as the Chair of the Rochester Section of IEEE in 1994–1995. He is a member of Sigma Xi.